J|A|C|S COMMUNICATIONS

Published on Web 03/16/2009

Highly Porous and Robust 4,8-Connected Metal−Organic Frameworks for Hydrogen Storage

Liqing Ma, David J. Mihalcik, and Wenbin Lin*

Department of Chemistry, CB#3290, University of North Carolina, Chapel Hill, North Carolina 27599

Received December 8, 2008; E-mail: wlin@unc.edu

Metal−organic frameworks (MOFs) have emerged as a class of very promising hybrid functional materials due to the ability to tune their properties in a modular fashion.[1] For example, a family of MOFs of the primitive cubic network (**pcu**) topology was systematically constructed from 6-connected $[Zn_4(\mu_4\text{-}O)(O_2CR)_6]$ secondary building units (SBUs) and 2-connected linear dicarboxylate bridging ligands of varied lengths to afford isoreticular porous materials with tunable pore/channel sizes, shapes, and functionalities.[2] Carboxylate-bridged copper paddle wheels represent another interesting SBU for the isoreticular synthesis of MOFs because of their enhanced stability over the $[Zn_4(\mu_4\text{-}O)(O_2CR)_6]$ SBUs. Indeed, the HKUST-1 with the framework formula of $[Cu_3(BTC)_2(H_2O)_3]$ that is built from copper paddle-wheel SBUs still serves as a benchmark material in both stability and gas uptake capacity.[3] However, the lower connectivity (4) of the paddle-wheel SBU makes it difficult to implement the isoreticular synthesis. For example, when copper paddle wheels are combined with readily available linear dicarboxylate bridging ligands, 2-D networks are expected based on topological considerations. We and others have recently demonstrated the ability to construct 4,4-connected MOFs of the PtS and related topology based on copper paddle wheels and tetracarboxylate bridging ligands.[4,5] We are particularly interested in designing robust MOFs based on aromatics-rich bridging ligands for gas storage applications.[6] The use of elongated aromatic tetracarboxylate bridging ligands has however led to severe framework distortion of these MOFs upon solvent removal which significantly reduces the porosity and negatively impacts the gas uptake capacity.[4] Herein we wish to report a new strategy to rigidify the frameworks by constructing 4,8-connected MOFs of the **scu** topology based on copper paddle wheels and aromatics-rich octacarboxylic acid bridging ligands.

The new enantiopure 1,1′-binaphthyl-derived *octa*-carboxylic acid ligand (*R*)-$\mathbf{L_1}$-H_8 was synthesized by a Pd-catalyzed Suzuki coupling between (*R*)-4,4′,6,6′-tetrabromo-2,2′-diethoxy-1,1′-binaphthyl and dimethyl-5-(pinacolboryl)isophthalate followed by base-catalyzed hydrolysis. (*R*)-$\mathbf{L_2}$-H_8 was obtained by deprotecting the ethoxy groups of the methyl ester of (*R*)-$\mathbf{L_1}$-H_8 using BBr_3 in CH_2Cl_2. (*R*)-$\mathbf{L_3}$-H_8 was synthesized in a similar fashion as (*R*)-$\mathbf{L_1}$-H_8 except 4,4′,6,6′-tetrabromo-2,2′-dibenzyloxy-1,1′-binaphthyl was used. All of the intermediates and ligands were characterized by NMR spectroscopy and high-resolution mass spectrometry.

Single crystals of $[Cu_4(\mathbf{L_1})(H_2O)_4]\cdot 12DEF\cdot 2H_2O$ (**1**), $[Cu_4(\mathbf{L_2})(H_2O)_4]\cdot 14DMF\cdot 2H_2O$ (**2**), and $[Cu_4(\mathbf{L_3})(H_2O)_4]\cdot 8DMF\cdot 12H_2O$ (**3**) were obtained by treating $\mathbf{L_1}$-H_8, $\mathbf{L_2}$-H_8, or $\mathbf{L_3}$-H_8 with Cu(II) salts in diethylformamide (DEF) or dimethylformamide (DMF) at elevated temperatures, respectively. The formulas of **1**−**3** were established by single crystal X-ray structure determination, ^{1}H NMR spectroscopy, and TGA analyses. Single crystal X-ray diffraction studies unambiguously established the framework structures of **1**−**3**, whereas the combination of ^{1}H NMR studies and TGA analyses gave the compositions of the included solvate molecules in **1**−**3**.

Scheme 1

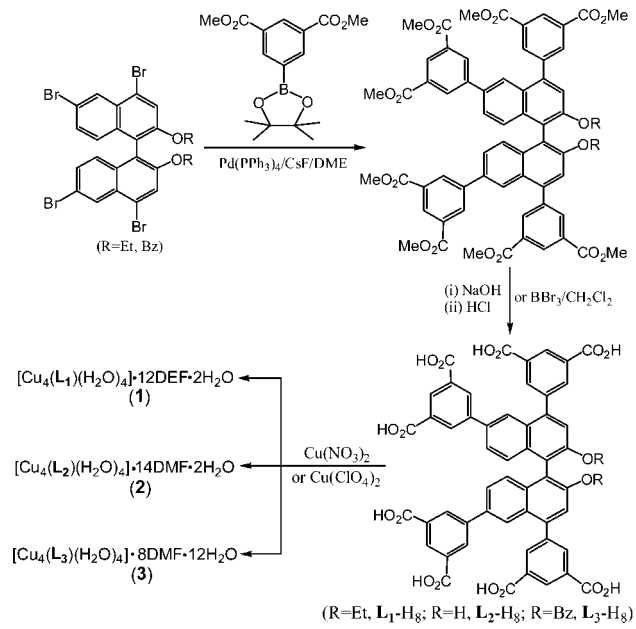

Compound **1** crystallizes in the tetragonal *P*4 space group with two copper atoms, one-half $\mathbf{L_1}$ ligand, and two water molecules for the framework in the asymmetric unit.[7] The Cu atoms coordinate to four carboxylate oxygen atoms of four different $\mathbf{L_1}$ ligands to form $[Cu_2(O_2CR)_4]$ paddle wheels that are shown as red rectangles in Figure 1a. Each Cu atom also coordinates to a terminal water molecule in the axial position. The $\mathbf{L_1}$ ligand is linked to eight copper paddle wheels via the bridging carboxylate groups in a rectangular prismatic fashion. The copper paddle wheels thus serve as 4-connected nodes, whereas the $\mathbf{L_1}$ ligands act as 8-connected nodes, and as a result, **1** adopts the known but very rare (4,8)-connected **scu** topology with the Schläfli symbol $\{4^4\cdot 6^2\}_2\{4^{16}\cdot 6^{12}\}$ (Figures 1b and S18).[8] Compound **1** represents only the third MOF with the **scu** topology and the first one that is built from an 8-connected bridging ligand.[9]

We obtained a similar crystalline MOF **1′** when racemic $\mathbf{L_1}$-H_8 was used in place of (*R*)-$\mathbf{L_1}$-H_8.[10] Interestingly, single crystal X-ray structure determination showed that the racemic $\mathbf{L_1}$-H_8 self-resolved during the MOF growth to give single crystals of **1′** that contained racemically twinned domains. The structure of **1′** is thus the same as that of **1** with the exception of racemic twinning.

Compounds **2** and **3** are isostructural to compound **1** with essentially identical cell parameters.[11] Because of the elongated $\mathbf{L_1}$−$\mathbf{L_3}$ ligands, **1**, **2**, and **3** possess very large solvent accessible volumes of 61.0%, 64.7%, and 52.7% of the unit cell volume as calculated by PLATON,[12] respectively. Consistent with this, **1**, **2**, and **3** exhibited a significant TGA solvent weight loss of 51%, 49%,

10.1021/ja809590n CCC: $40.75

and 39% in the 25−280 °C temperature range, respectively. As shown in Figure 1e and 1f, compound **2** possess square channels of ~7 × 7 Å along the *c* axis and rectangular channels of ~5.3 × 10.6 Å along the (110) direction. The ethoxy groups of the $\mathbf{L_1}$ ligands protrude into the open channels that run along the *c* axis and the (110) direction in **1**, thus reducing the open channel sizes. As expected, the bulkier benzyloxy groups in **3** reduce the open channel sizes even further, with the open channel of ~7 × 4 Å along the *c* axis (Figure 1g) and the open channels of ~5.3 × 4.4 Å and 4.0 × 2.4 Å along the (110) direction due to the protruding benzyloxy groups (Figure 1h).

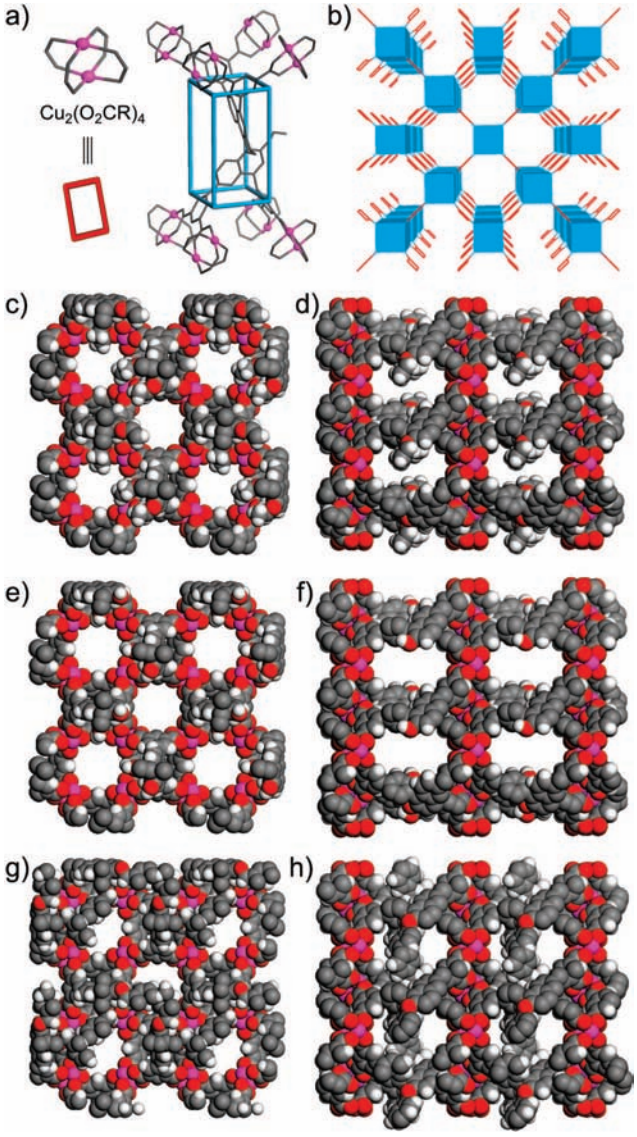

Figure 1. (a) A view of $[Cu_2(O_2CR)_4]$ paddle wheels (represented as red rectangles) and their connectivity with the $\mathbf{L_1}$ ligand (represented as a blue rectangular prism) in **1**. (b) A simplified connectivity scheme of **1** showing the **scu** topology. (c) Space-filling model of **1** as viewed down the *c* axis, showing irregular open channels with the largest dimension of ~7 Å. (d) Space-filling model of **1** as viewed along the (110) direction, showing irregular channels with the largest dimension of 10.6 Å. (e) Space-filling model of **2** as viewed down the *b* axis, showing square open channels of ~7 Å in each side. (f) Space-filling model of **2** as viewed along the (110) direction, showing rectangular channels of ~5.3 × 10.6 Å. (g) Space-filling model of **3** as viewed down the *c* axis, showing open channels of ~7 × 4 Å. (h) Space-filling model of **3** as viewed along the (110) direction, showing two different open channels of ~5.3 × 4.4 Å and 4.0 × 2.4 Å.

The permanent porosity of **1**, **2**, and **3** was established by nitrogen adsorption at 77 K. After activation at 60 °C under vacuum, **1** exhibited a Langmuir surface area of 2486 m^2/g (Figure 2) whereas **2** exhibited a Langmuir surface area of 2650 m^2/g. Compound **3** exhibited a significantly lower Langmuir surface area of 1841 m^2/g. BET surface areas are 2149, 2285, and 1605 m^2/g for **1**, **2**, and **3**, respectively.[13] This porosity trend is entirely consistent with the increasing steric bulk of hydroxy, ethoxy, and benzyloxy groups on the 2,2′-position of the binaphthyl moieties of the octa-carboxylic acid bridging ligands.

Notably, the experimental surface areas of **1** and **2** perfectly agree with those calculated using the simulated N_2 adsorption isotherms; grand canonical Monte Carlo (GCMC) simulations[14] gave calculated Langmuir surface areas of 2502 and 2592 m^2/g for **1** and **2**, respectively. The GCMC simulation of **3** gave a slightly higher Langmuir surface area of 2134 m^2/g than the experimental result (1841 m^2/g). This discrepancy could be caused by the flexible (and disordered) nature of the bulky benzyloxy groups. Upon desolvation, the benzyloxy group can move around to generate a portion of pores that are smaller than the dynamic diameter of adsorbate molecules (N_2). The GCMC simulation, on the other hand, assumes a rigid orientation of the protruding benzyloxy groups and gives the idealized surface area. The N_2-inaccessible pores can account for the discrepancy between the experimental and GCMC simulated surface areas for **3**.

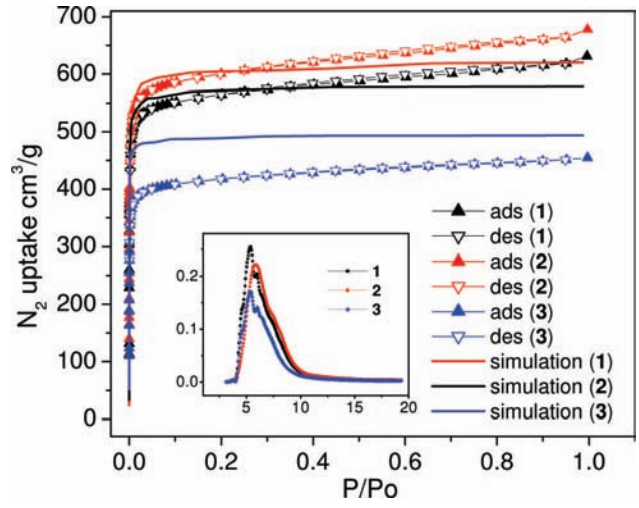

Figure 2. Experimental and calculated N_2 adsorption isotherms for **1** (black), **2** (red), and **3** (blue). Solid triangles (adsorption), open triangles (desorption), and solid lines (GCMC simulation results). Inset shows the pore size distributions (HK method) for **1** (black), **2** (red), and **3** (blue) with the *x* axis showing pore diameter in Å and the *y* axis showing Dv(w) in $cm^3/Å/g$.

The pore sizes of **2** have also slightly increased as compared to those of **1** (Figure 2 inset). This trend is consistent with the slightly less porous structure of **1** due to the steric bulk of the ethoxy groups. The pore sizes of **3** are however very similar to those of **1**, which is inconsistent with the steric difference between the ethoxy and benzyloxy groups. In fact, the pore sizes derived from GCMC simulated adsorption isotherm for **3** are smaller than those for **1** (Figure S36). This discrepancy between experimental and calculated pore sizes for **3** is presumably a result of the disordered nature of the bulky benzyloxy groups. Consistent with the porosity trend, the HK method cumulative pore volume is 0.92, 0.86, and 0.64 cc/g for **2**, **1**, and **3**, respectively.

As expected, the powder X-ray diffraction (PXRD) patterns of **1**, **2**, and **3** are very similar to each other, consistent with their

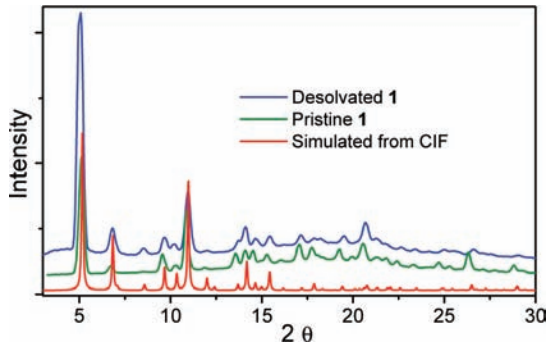

Figure 3. PXRD patterns of pristine (green) and evacuated (blue) sample of **1** along with calculated PXRD pattern (red).

isostructural nature. Furthermore, the PXRD patterns of the evacuated samples of **1**, **2**, and **3** are essentially the same as those of pristine **1**, **2**, and **3**, further demonstrating the maintenance of the framework structure upon solvent removal (Figure 3). This is in stark contrast with our earlier results which showed that the frameworks of 4,4-connected MOFs based on copper paddle-wheel SBUs and elongated tetracarboxylate bridging ligands severely distorted (as evidenced by the loss of PXRD peaks) to give experimental surface areas only a very small fraction of those calculated by GCMC simulations.[4] The higher connectivity of the $\mathbf{L_1}-\mathbf{L_3}$ ligands has apparently stabilized the frameworks of **1**−**3** against distortion (also called breathing in recent literatures[14]). The use of bridging ligands of high connectivity thus presents an alternative strategy to the reliance on high-nuclearity metal clusters for building highly stable and porous MOFs.[15]

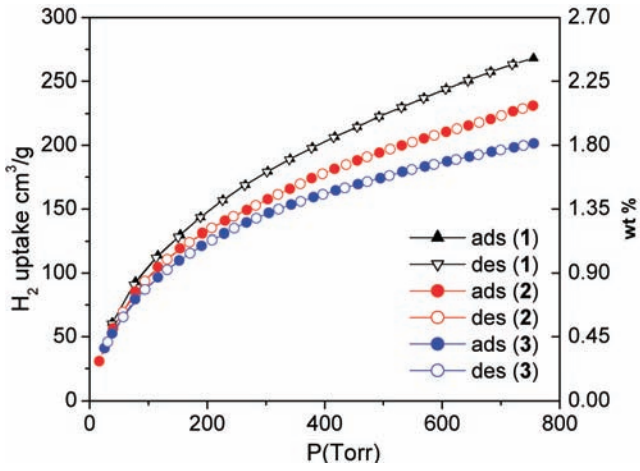

Figure 4. Experimental hydrogen adsorption isotherms of **1** (black), **2** (red), and **3** (blue). Solid triangles and circles (adsorption) and open triangles and circles (desorption).

Hydrogen adsorption experiments show **1** uptakes 2.5 wt% H_2 at 77 K and 1 atm (Figure 4), which is among the highest for MOFs at 1 atm.[16] In the volumetric sense, **1** has a H_2 uptake of 17.4 g/L, superior to other aromatics-rich MOFs (e.g., 5.34 g/L for MOF-177).[16] Despite having a higher surface area, **2** exhibits a lower hydrogen uptake of 2.1 wt%. This result is not entirely surprising as earlier work has shown that MOFs with smaller pore sizes tend to have higher hydrogen uptake capacities.[16] However, our intent to further reduce the pore size by using the bulkier benzyloxy groups did not yield the expected results. As mentioned earlier, the pore size distribution for **3** is essentially the same as that of **1**. Compound **3** exhibited an even lower hydrogen uptake of 1.8 wt%, probably as a result of its smallest surface area and pore volume. This work thus demonstrates the ability to tune the surface area, pore size, and gas uptake by systematically changing the alkoxy groups of the *octa*-carboxylic acid bridging ligands in **1**−**3**. Characterization of the saturation hydrogen uptake capacity of **1**−**3** is ongoing, and these results will be reported in a future publication.

In summary, we have constructed highly porous and robust (4,8)-connected MOFs based on new octa-carboxylate ligands and copper paddle-wheel SBUs. The new MOFs exhibit remarkable framework stability as a result of the high connectivity of the bridging ligands and show significant hydrogen uptake. This work thus represents a new approach toward designing highly porous, robust, tunable, and functional MOFs using multidentate bridging ligands of high connectivity.

Acknowledgment. We thank the NSF (DMR-0605923) for financial support. D.J.M. thanks the Department of Education for a GAANN fellowship.

Supporting Information Available: Experimental procedures, characterization data, and X-ray crystallographic files (CIF). This material is available free of charge via the Internet at http://pubs.acs.org.

References

(1) (a) Kitagawa, S.; Kitaura, R.; Noro, S. *Angew. Chem., Int. Ed* **2004**, *43*, 2334–2375. (b) Bradshaw, D.; Warren, J. E.; Rosseinsky, M. J. *Science* **2007**, *315*, 977–980. (c) Evans, O. R.; Lin, W. *Acc. Chem. Res.* **2002**, *35*, 511–522.
(2) Eddaoudi, M.; Kim, J.; Rosi, N.; Vodak, D.; Wachter, J.; O'Keeffe, M.; Yaghi, O. M. *Science* **2002**, *295*, 469–472.
(3) Chui, S. S. Y.; Lo, S. M. F.; Charmant, J. P. H.; Orpen, A. G.; Williams, I. D. *Science* **1999**, *283*, 1148–1150.
(4) (a) Ma, L.; Lee, J. Y.; Li, J.; Lin, W. *Inorg. Chem.* **2008**, *47*, 3955–3957. (b) Wu, S.; Ma, L.; Long, L.-S.; Zheng, L.-S.; Lin, W. *Inorg. Chem.* **2009**, *48*, 2436–2442. (c) Ma, L.; Lin, W. *J. Am. Chem. Soc.* **2008**, *130*, 13834–13835.
(5) Lin, X.; Jia, J. H.; Zhao, X. B.; Thomas, K. M.; Blake, A. J.; Walker, G. S.; Champness, N. R.; Hubberstey, P.; Schröder, M. *Angew. Chem., Int. Ed.* **2006**, *45*, 7358–7364.
(6) Kesanli, B.; Cui, Y.; Smith, M. R.; Bittner, E. W.; Bockrath, B. C.; Lin, W. *Angew. Chem., Int. Ed.* **2005**, *44*, 72–75.
(7) Crystal data for **1**: Tetragonal, *P*4, $a = 18.272(1)$ Å, $c = 17.091(1)$ Å, $V = 5705.9(2)$ Å^3, $\rho_{calcd} = 0.751$ g/cm^3. R1 = 0.056, *w*R2 = 0.147. Flack parameter = 0.10(5).
(8) Blatov, V. A.; Peskov, M. V. *Acta Cystallogr., Sect. B* **2006**, *62*, 457–466.
(9) (a) Sra, A. K.; Rombaut, G.; Lahitête, F.; Golhen, S.; Ouahab, L.; Mathonière, C.; Yakhmi, J. V.; Kahn, O. *New. J. Chem.* **2000**, *24*, 871–876. (b) Duan, X.; Chen, X.; Lin, J.; Zang, S.; Li, Y.; Zhu, C.; Meng, Q. *CrystEngComm* **2008**, *10*, 706–714.
(10) Crystal data for **1′**: Tetragonal, *P*4, $a = 18.296(1)$ Å, $c = 17.110(1)$ Å, $V = 5727.4(2)$ Å^3, $\rho_{calcd} = 0.748$ g/cm^3. R1 = 0.055, *w*R2 = 0.152 ($I > 2\sigma(I)$). Flack parameter = 0.47(6).
(11) Crystal data for **2**: Tetragonal, *P*4, $a = 18.0725(9)$ Å, $c = 17.1854(11)$ Å, $V = 5613.0(2)$ Å^3, $\rho_{calc} = 0.735$ g/cm3. R1 = 0.064, *w*R2 = 0.142. Flack parameter = 0.01(1). Crystal data for **3**: Tetragonal, *P*4, $a = 18.0648(12)$ Å, $c = 17.1132(12)$ Å, $V = 5584.7(5)$ Å^3, $\rho_{calcd} = 0.839$ g/cm^3. R1 = 0.077, *w*R2 = 0.190. Flack parameter = 0.27(14).
(12) Spek, A. L. *J. Appl. Crystallogr.* **2003**, *36*, 7–13.
(13) The Langmuir and BET surface areas were calculated from the pressure range of $P/P_0 = 0.001-0.30$ and $0.01-0.10$, respectively. All of the BET plots have large negative BET constants, indicating no multilayer adsorption. The Langmuir model is thus more appropriate for **1**−**3**. See Supporting Information for detailed analyses. Walton, K. S.; Snurr, R. Q. *J. Am. Chem. Soc.* **2007**, *129*, 8552–8556.
(14) (a) Serre, C.; Millange, F.; Thouvenot, C.; Noguès, M.; Marsolier, G.; Louër, D.; Férey, G. *J. Am. Chem. Soc.* **2002**, *124*, 13519–13526. (b) Llewellyn, P. L.; Maurin, G.; Devic, T.; Loera-Serna, S.; Rosenbach, N.; Serre, C.; Bourrelly, S.; Horcajada, P.; Filinchuk, Y.; Férey, G. *J. Am. Chem. Soc.* **2008**, *130*, 12808–12814.
(15) Cavka, J. H.; Jakobsen, S.; Olsbye, U.; Guillou, N.; Lamberti, C.; Bordiga, S.; Lillerud, K. P. *J. Am. Chem. Soc.* **2008**, *130*, 13850–13851.
(16) (a) Mircea, D.; Long, J. R. *Angew. Chem., Int. Ed.* **2008**, *47*, 6766–6779. (b) Zhao, D.; Yuan, D.; Zhou, H-C. *Energy Environ. Sci.* **2008**, *1*, 222–235. (c) Rowsell, J. L. C.; Yaghi, O. M. *Angew. Chem., Int. Ed.* **2005**, *44*, 4670–4679. (d) Farha, O. K.; Spokoyny, A. M.; Mulfort, K. L.; Hawthorne, M. F.; Mirkin, C. A.; Hupp, J. T. *J. Am. Chem. Soc.* **2007**, *129*, 12680–12681.

JA809590N